IEEE Access
Multidisciplinary | Rapid Review | Open Access Journal

Received November 17, 2019, accepted December 26, 2019, date of publication January 6, 2020, date of current version January 22, 2020.

Digital Object Identifier 10.1109/ACCESS.2020.2964106

Rotor Vibration Control of a Bearingless Induction Motor Based on Unbalanced Force Feed-Forward Compensation and Current Compensation

HUIMIN ZHU[1], ZEBIN YANG[1], XIAODONG SUN[2], (Senior Member, IEEE), DING WANG[1], AND XI CHEN[1]

[1]School of Electrical and Information Engineering, Jiangsu University, Zhenjiang 212013, China
[2]Automotive Engineering Research Institute, Jiangsu University, Zhenjiang 212013, China

Corresponding authors: Zebin Yang (zbyang@ujs.edu.cn) and Xiaodong Sun (xdsun@ujs.edu.cn)

This work was supported in part by the Natural Science Foundation of China under Project 51475214 and Project 51875261, in part by the Natural Science Foundation of Jiangsu Province of China under Project BK20180046 and Project BK20170071, in part by the Priority Academic Program Development of Jiangsu Higher Education Institutions, and in part by the High-Tech Key Laboratory of Agricultural Equipment and Intelligence of Jiangsu Province.

ABSTRACT To handle the unbalanced vibration caused by uneven rotor mass distribution in a bearingless induction motor (BIM), a control strategy that integrates unbalanced feed-forward compensation and current compensation is presented. Firstly, based on the analysis of the BIM rotor vibration mechanism and the unbalanced vibration influence on the performance of the BIM, the dynamic model of the rotor is derived. Secondly, an unbalanced force feed-forward compensation controller is designed to extract the synchronous vibration signals through the synchronous signal detection unit, and then the compensation force components are generated by unbalanced feed-forward compensation controller. In addition, considering the influence of current in the rotor induced by suspension winding, a current compensation link is applied to the system to enhance the suspension performance. Finally, a rotor unbalanced vibration compensation control system of the BIM is established. The simulation and experimental results show that the proposed compensation control strategy not only can effectively reduce the rotor radial displacement and suppress the unbalanced vibration, but also can improve the suspension performance.

INDEX TERMS Bearingless induction motor (BIM), current compensation, feed-forward compensation, radial displacement, rotor eccentricity.

I. INTRODUCTION

A bearingless motor is a new type of motor which breaks through the balance of air-gap magnetic field of the traditional motor to produce electromagnetic torque and radial suspension force. Using the structure similarity between the magnetic bearing and the motor stator, two sets of different pole-pair windings are embedded in the bearingless motor to destroy the symmetry of air-gap magnetic field, which produces electromagnetic torque and radial suspension force and realizes the functions of rotor rotation and suspension [1]–[6].

The associate editor coordinating the review of this manuscript and approving it for publication was Feifei Bu.

Compared with other types of bearingless motors, the bearingless induction motor (BIM) not only contains the advantages of the conventional induction motor, such as simple structure, low pulsating torque and easy flux-weakening control, but also inherits the advantages of the magnetic bearing, such as no contact, no abrasion, no lubrication, no pollution and long service life [7]–[11]. These advantages can make the BIM popular in the special drive fields including high-speed, ultra-high speed, vacuum, clean and corrosion environment [12]–[16]. Furthermore, the BIM has become one of the hot spots in the research fields of bearingless motors presently.

However, in the manufacturing and actual operation of the BIM, the rotor vibration will be inevitably caused by

This work is licensed under a Creative Commons Attribution 4.0 License. For more information, see http://creativecommons.org/licenses/by/4.0/

uneven mass distribution of the rotor lamination, the problem of machining precision and the deformation of the rotating shaft in long-term vibration [17]–[20]. Next, the geometric center axis and the inertia axis of the rotor are difficult to coincide completely. Therefore, an exciting force acting on the rotor will be produced during the operation of the motor, which has the same frequency with the speed and is proportional to the square of the speed [21]–[23]. When the motor reaches a certain speed, a large unbalanced vibration will be caused even the offset is small. If the unbalanced vibration exceeds the limit of air-gap, it will directly lead to the failure of the rotor suspension. It not only restricts the further increase of the speed, but also seriously affects the safe operation of the BIM. In addition, the vibration signal detected by displacement sensors may result in the current saturation in the power amplifier, thus affecting the entire control loop [24]. Therefore, the research on the unbalanced rotor vibration suppression of the BIM is of great theoretical and practical significance.

Recently, for the unbalanced rotor vibration of bearingless motors, scholars at home and abroad have put forward many vibration suppression methods based on the control theory [25]–[30]. Most of these methods are divided into two categories: minimum current control and minimum displacement control. In [31], a compensation control strategy of radial suspension force is proposed based on the characteristics of different decoupling strategies. However, the strategy is greatly influenced by the change of motor parameters, which leads to the decrease of control accuracy. In [32], a novel axial vibration suppression strategy for a two-axis actively positioned permanent magnet bearingless motor is proposed. The strategy can increase the damping force by adjusting the d-axis current to realize the active suspension control in the axial direction of the rotor. Moreover, the rotor axial position is estimated by the flux-linkage variation of the motor winding, so the additional displacement sensor is not necessary. In [33], a rotor adaptive vibration suppression control strategy based on multi-frequency tracking algorithm is proposed. This algorithm can accurately and effectively identify the frequency of vibration signals, but the algorithm used in the strategy is complicated and difficult to realize. In [34], a feed-forward compensation control strategy of the BIM based on the coordinate transformation is proposed to effectively reduce the rotor vibration. However, the vibration displacement used as the compensation signal is just an open-loop compensation for the suspension system, thus leading to the low control precision. In [35], the adaptive least-mean-square (LMS) filter is utilized to generate the vibration compensation signal, which reduces the eccentric vibration amplitude of the rotor and improves the suspension accuracy. However, it is difficult to determine the step parameters of the adaptive filter, so the convergence speed and filtering effect can be affected.

In view of the radial offset and unbalanced vibration caused by uneven rotor mass, a control strategy that integrates unbalanced force feed-forward compensation and current compensation is proposed. Compared with the existing control methods, this strategy has the advantages of simple control structure and remarkable control effects. As the control system is adjusted by traditional PID control, it is difficult to meet the high-performance control requirements of the BIM nonlinear system, which needs further improvement in future research [36], [37]. In this strategy, the feed-forward compensation controller is applied to the suspension control system, the synchronous signal processor is utilized to extract the synchronous component of the displacement signal and the synchronous component is converted to weaken the unbalanced exciting force. Meanwhile, the suspension control system ignores the induced current of the suspension winding in the rotor [38], so the magnitude of the radial suspension force is changed, which has certain influences on the unbalanced vibration. The neglected rotor induced current is taken into account by the current compensation link. Since the rotor current is difficult to measure, the stator current component of the suspension winding can be obtained by means of elimination, thus the suspension performance of the rotor can be effectively improved and the radial displacement can be reduced. The simulation control model of vibration compensation is established by MATLAB/Simulink and the simulations are carried out at different speeds, taking low speed (3000r/min) and medium-high speed (8000r/min) as examples in the paper. In addition, the experimental research is also conducted on the experimental platform of the BIM. The simulation and experimental results show that the proposed vibration suppression strategy can achieve good suspension effects, which not only realizes the stable suspension in a wide speed range, but also reduces the radial offset caused by the rotor vibration of the BIM.

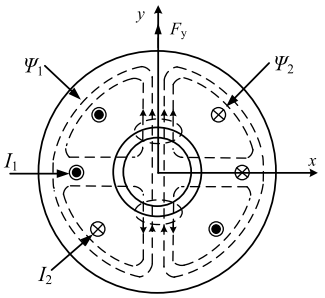

FIGURE 1. Principle of radial suspension forces.

II. PRINCIPLE AND MATHEMATICAL MODEL OF THE BIM

A. THE PRINCIPLE OF THE BIM RADIAL SUSPENSION FORCE

The BIM is embedded a set of suspension winding in the stator of conventional induction motor. Through the interaction of magnetic fields of two sets of different pole-pair windings, the symmetry of the original air-gap magnetic field is broken and radial suspension forces are generated to achieve the suspension of the rotor [8], [39]. The pole-pairs of torque winding and suspension winding in the motor stator slot are

P_M and P_B, respectively, and the corresponding electrical angular frequencies are ω_1 and ω_2. If two sets of windings meet the following condition: (1) $P_B = P_M \pm 1$; (2) $\omega_1 = \omega_2$, the controllable radial suspension forces can be generated [40], [41]. Fig.1 shows the principle of generating the radial suspension forces on the BIM. The pole-pairs of the torque winding and the suspension winding are $P_M = 1$ and $P_B = 2$, respectively. When two sets of windings are respectively supplied with currents I_1 and I_2, a two-pole flux-linkage Ψ_1 and a four-pole flux linkage Ψ_2 are produced. At this point, the air-gap magnetic fields on the upper side are in the same direction, the magnetic density increases, while the air-gap magnetic fields on the lower side are in the opposite direction, the magnetic density decreases. Therefore, the radial suspension force F_y is produced along the y-axis. Through the above analysis, the controllable radial suspension forces both in x-axis and y-axis can be obtained by changing the magnitude and direction of currents I_1 and I_2.

B. MATHEMATICAL MODEL OF THE BIM

The radial suspension forces of the BIM in the x, y directions that are derived from Maxwell tensor method can be expressed as [42]–[44]:

$$\begin{cases} F_x = K(\Psi_{1d} i_{s2d} + \Psi_{1q} i_{s2q}) \\ F_y = K(\Psi_{1d} i_{s2q} - \Psi_{1q} i_{s2d}) \end{cases} \tag{1}$$

where $K = K_l + K_m$ is a constant, K_l is the Lorentz force constant, and K_m is the Maxwell force constant;$K_l = \frac{N_2 P_1}{2rN_1}$, $K_m = \frac{\pi L_{2m} P_1^2 P_2^2}{18 N_1 N_2 \mu_0 l r}$. Among them, Ψ_{1d} and Ψ_{1q} are the air gap flux linkage components of the torque winding in the d-q coordinate system; i_{s2d} and i_{s2q} are the stator current components of the suspension winding in the d-q coordinate system; N_1 and N_2 are the effective turns of the torque winding and suspension winding; P_1 and P_2 are the pole-pairs of the torque winding and the suspension winding; r is the outer diameter of the rotor; L_{2m} is the mutual inductance of the suspension winding; μ_0 is the vacuum permeability; l is the effective length of the shaft.

Electromagnetic torque equation is

$$T_e = P_1(\Psi_{1d} i_{s1q} - \Psi_{1q} i_{s1d}) \tag{2}$$

Flux linkage equation is

$$\begin{cases} \Psi_{s2d} = L_{s2l} i_{s2d} + \Psi_{2d} \\ \Psi_{s2q} = L_{s2l} i_{s2q} + \Psi_{2q} \\ \Psi_{r2d} = L_{r2l} i_{r2d} + \Psi_{2d} \\ \Psi_{r2q} = L_{r2l} i_{r2q} + \Psi_{2q} \end{cases} \tag{3}$$

Voltage equation is

$$\begin{cases} U_{s2d} = R_{s2} i_{s2d} + p\Psi_{s2d} - \Psi_{s2q}\omega_p \\ U_{s2q} = R_{s2} i_{s2q} + p\Psi_{s2q} + \Psi_{s2d}\omega_p \\ U_{r2q} = R_{r2} i_{r2q} + p\Psi_{r2q} + \Psi_{r2d}\omega_s \\ U_{r2d} = R_{r2} i_{r2d} + p\Psi_{r2d} - \Psi_{r2q}\omega_s \end{cases} \tag{4}$$

where i_{s1d} and i_{s1q} are the stator current components of the torque winding in the d-q coordinate system; Ψ_{s2d}, Ψ_{s2q}, Ψ_{r2d} and Ψ_{r2q} are the flux linkage components of the suspension winding in d-q coordinates, respectively; L_{s2l} and L_{r2l} are the stator and rotor leakage inductance of the suspension winding; i_{s2d}, i_{s2q}, $i_{r2d}$and i_{r2q} are the current components of the suspension winding in d-q coordinates; $\Psi_{2d}$and Ψ_{2q} are the air gap flux linkage components of the suspension winding in d-q coordinates; U_{s2d}, U_{s2q}, $U_{r2d}$and U_{r2q} are the voltage components of the suspension winding in d-q coordinates, respectively; R_{s2} and R_{r2} are resistances of the stator and rotor of the suspension winding; p is a differential operator; $\omega_p$and ω_s are the air gap magnetic field velocity and the slip angular velocity, respectively.

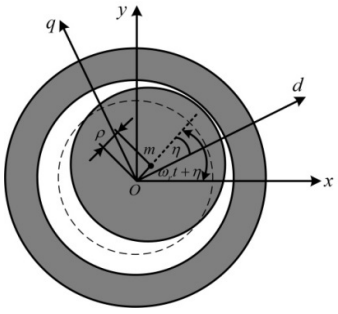

FIGURE 2. Schematic diagram of the rotor eccentricity.

III. ANALYSIS OF ROTOR VIBRATION MECHANISM

The diagram of the rotor eccentricity is shown in Fig.2, where ρ represents the eccentricity between the centroid of the rotor and the geometric center; ω_r is the mechanical angular velocity of the rotor; η is the initial direction angle of the centroid of the rotor. Ideally, the centroid m coincides with the geometric center O, the rotor will not deviate during the operation of the motor. The suspension control system only provides the radial suspension force to support the weight of the rotor and load. When the centroid of the rotor is not at the geometric center, that is, the eccentricity ρ is generated, the rotor vibration will be strengthened with the increase of the motor speed, the vibration displacement will also accordingly increase, which seriously affect the suspension performance of the motor.

As shown in Fig.2, when the rotor revolves around the center axis with the angular velocity ω_r, the centrifugal force that synchronously changes with the rotor position will be generated on the rotor. Its components on the x, y axis are described as:

$$F_{cx} = M\rho\omega_r^2 \cos(\omega_r t + \eta) \tag{5}$$

$$F_{cy} = M\rho\omega_r^2 \sin(\omega_r t + \eta) \tag{6}$$

When there is no mass eccentricity in the rotor, according to Newton's law, the dynamic equations of the rotor in the x, y directions are obtained as:

$$M\ddot{x} + c_x\dot{x} + k_x x = F_x - f_{Mx} \tag{7}$$

$$M\ddot{y} + c_y\dot{y} + k_y y = F_y - f_{My} \tag{8}$$

where M is the mass of the rotor; c_x and c_y are the coupling parameters of the rotor; k_x and k_y are the stiffness coefficients of the rotor; F_x and F_y are the radial suspension forces in the x, y directions; f_{Mx} and f_{My} are the components of rotor weight and external loads in the x, y directions.

When the eccentricity of the rotor is taken into account, the dynamic equations of the rotor in the x, y directions can be rewritten as:

$$M\ddot{x} + c_x\dot{x} + k_x x = M\rho\omega_r^2\cos(\omega_r t + \eta) + F_x - f_{Mx} \quad (9)$$

$$M\ddot{y} + c_y\dot{y} + k_y y = M\rho\omega_r^2\sin(\omega_r t + \eta) + F_y - f_{My} \quad (10)$$

For dynamic equations (9) and (10), the displacement response of the BIM is derived as:

$$\begin{cases} x = x_0\cos(\omega_r t + \eta - \delta_1) + \Delta x - \dfrac{f_{Mx}}{k_x} \\ y = y_0\sin(\omega_r t + \eta - \delta_2) + \Delta y - \dfrac{f_{My}}{k_y} \end{cases} \quad (11)$$

where x_0 and y_0 are the displacement amplitudes along the x and y axis due to the rotor eccentricity, respectively; δ_1 and δ_2 are the angles associated with the rotor speed, rotor mass, coupling parameters and stiffness coefficients; Δx and Δy are the uncertain displacements caused by F_x and F_y, respectively, when the actual suspension force is basically the same as the given suspension force, Δx and Δy are very small.

It is known from the formula (11) that the displacement response of the BIM is composed of the sinusoidal components and some uncertain displacements. These sinusoidal components have the same frequency with the speed. The rotor will deviate from the geometric center to generate periodic and unbalanced vibration under the impact of centrifugal force. If no measures are taken to reduce this vibration, the radial displacement of the rotor will be increased and the suspension performance will be deteriorated, which eventually results in the failure of suspension. Therefore, a control strategy that integrates unbalanced force feed-forward compensation and current compensation is used to compensate for the unbalanced vibration and reduce the vibration amplitude of the rotor, so that the suspension performance is effectively improved.

IV. ROTOR VIBRATION SUPPRESSION OF THE BIM

A. FEED-FORWARD COMPENSATION FOR UNBALANCED FORCE

To suppress the vibration caused by uneven rotor mass distribution, it is necessary to reduce the periodic component of the same frequency as the rotor by means of active control in the suspension system. In this paper, the unbalanced force feed-forward compensation control strategy is used to detect the displacement signal of the same frequency from the initial signal. The unbalanced compensation control force is produced by coordinate transformation, PID modulation, filtering and other operations to make the rotor rotate around its geometric center axis, so that the radial offset of the rotor is reduced.

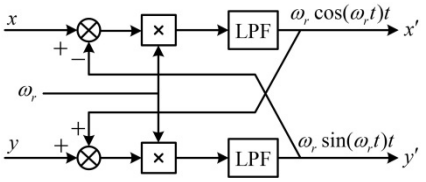

FIGURE 3. Synchronous signal detection process.

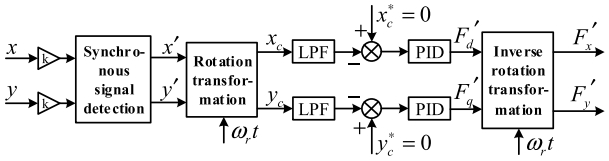

FIGURE 4. Unbalanced force feed-forward compensation controller.

To realize the unbalanced force compensation for the rotor vibration of the BIM, it is essential to extract the synchronous signals from the signals detected by radial displacement sensor. For this reason, a synchronization signal detection method with simple implementation and strong anti-interference is proposed, which is shown in Fig.3.

According to the formula (11), since the uncertain displacement components are very small and can be neglected. Generally, it is assumed that the stiffness of the BIM rotor is equal in horizontal and vertical directions and it is large enough. Therefore, the amplitude of the same frequency vibration signal generated on horizontal x-axis and vertical y-axis will be approximately the same and the rotor trajectory is approximately a circle. So the sinusoidal components of the same frequency as the speed are expressed as:

$$\begin{cases} x = A\cos(\omega_r t) \\ y = A\sin(\omega_r t) \end{cases} \quad (12)$$

$$\begin{cases} x' = A\omega_r\cos(\omega_r t)t \\ y' = A\omega_r\sin(\omega_r t)t \end{cases} \quad (13)$$

As can be seen from Fig.3, if the input sinusoidal signal is integrated and the speed is effectively identified, the input signal can be tracked accurately by the synchronous signal detection method, and then the other different frequency signals and random signals are filtered through the low-pass filter, and the synchronous signal of the same frequency as the rotational speed can be finally extracted.

The structure of the unbalanced force feed-forward compensation controller is shown in Fig. 4, where k is the adjustment coefficient of the synchronous signal. The synchronization signals x' and y' are obtained by synchronization signal detection unit from the initial displacement signals x and y. After the rotational transformation, the signal of the same frequency in the original displacement signal is changed into the DC quantity x_c, y_c and some high-frequency components in the synchronous rotating coordinate system, and then the high-frequency components are filtered through

the low-pass filter.

$$\begin{cases} x_c = x' \cos(\omega_r t) + y' \sin(\omega_r t) \\ y_c = -x' \sin(\omega_r t) + y' \cos(\omega_r t) \end{cases} \tag{14}$$

If the rotor reaches a stable suspension state, the radial offset of the rotor should be approximately equal to zero. The closed-loop control with zero error is carried out between the displacement signal output from the filter and the synchronization signal. Then, the unbalance compensation components F'_x, F'_y are obtained by PID modulation and inverse rotational transformation.

$$\begin{cases} F'_x = F'_d \cos(\omega_r t) - F'_q \sin(\omega_r t) \\ F'_y = F'_d \sin(\omega_r t) + F'_q \cos(\omega_r t) \end{cases} \tag{15}$$

Finally, the controller is applied to the suspension control system to suppress the rotor vibration.

When the rotor mass is unbalanced, the rotor will deviate from the geometric central axis under the action of centrifugal force. In this case, the compensation force produced in Fig.4 forcibly constrains the rotor to rotate around the geometric central axis and controls the vortex radius of the rotor to a relatively high precision. The feed-forward controller in this paper is designed based on the intrinsic characteristics of unbalanced interference force. It does not need specialized structures such as estimator and state observer, and can also successfully achieve the purpose of compensating for unbalanced interference. In addition, the implementation of the feedforward compensation controller no longer requires the accurate mathematical models of the rotor and unbalanced interference forces.

B. CURRENT COMPENSATION CONTROL

In the BIM, the magnitude of the induced current is related to the number of turns in the winding and the relationship between the number of turns of suspension winding and torque winding is about 1:10. Although the current values of the two sets of windings are the same, the induced current generated by the suspension winding in the rotor is generally neglected. However, the neglected induced current can result in changes in the magnitude of the radial suspension force and the unbalanced vibration. Therefore, an induced current compensation control strategy is proposed to consider the influence of induced current.

The suspension winding current breaks the balance of the original magnetic field of the motor, so that the magnetic field in one side of the air-gap is enhanced, while that in the other side is opposite. The generated Maxwell force will point to the side of the enhanced magnetic field. That is, the combination of the torque winding and the suspension winding produces the radial suspension forces. The stator current components of the suspension winding can be directly measured in the d-q coordinate system, while the rotor current is not available. Therefore, the rotor currents in formula (3) and (4) can be eliminated by the suspension winding model. Then, the relationship between the stator currents i_{s2d}, i_{s2q} and the currents i_{2d}, i_{2q} of the suspension system can be obtained as:

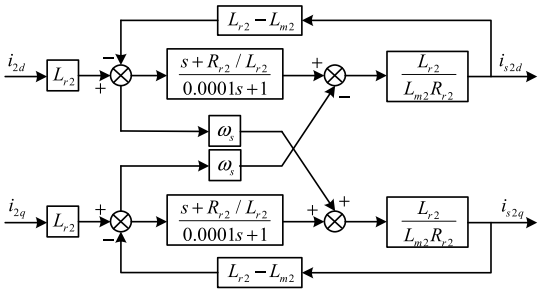

FIGURE 5. Current compensation link.

$$\begin{cases} i_{2d} = \dfrac{(\frac{R_{r2}}{L_{r2}}+p)}{L_{r2}[(\frac{R_{r2}}{L_{r2}}+p)^2+\omega_s^2]} \\ \times [i_{s2d}(R_{r2}\dfrac{L_{m2}}{L_{r2}}+L_{r2l}) + i_{s2q}\dfrac{\omega_s R_{r2} L_{m2}}{R_{r2}+pL_{r2}}] \\ i_{2q} = \dfrac{(\frac{R_{r2}}{L_{r2}}+p)}{L_{r2}[(\frac{R_{r2}}{L_{r2}}+p)^2+\omega_s^2]} \\ \times [i_{s2q}(R_{r2}\dfrac{L_{m2}}{L_{r2}}+L_{r2l}) - i_{s2d}\dfrac{\omega_s R_{r2} L_{m2}}{R_{r2}+pL_{r2}}] \end{cases} \tag{16}$$

According to formula (16), the relationship between i_{s2d}, i_{s2q} and i_{2d}, i_{2q} is shown in Fig.5, where s stands for the Laplacian.

As shown in Fig.5, considering the influence of the induced current produced by the suspension winding, the stator current components of the suspension winding can be obtained by means of elimination method to eliminate the rotor induced currents which are difficult to measure. In the paper, the control of radial suspension force is mainly achieved by controlling the suspension currents. Compared with the case that the induced currents are not taken into account, the suspension winding currents are compensated after considering the rotor induced currents. Then, the suspension winding currents are applied to the control system to directly affect the motor operation. Thus the suspension performance of the rotor is effectively improved and the control precision of the system is also increased.

V. SIMULATION AND EXPERIMENTAL ANALYSIS

A. RESULTS AND ANALYSIS OF THE SIMULATION

To verify the effectiveness of the compensation control strategy, a simulation model of the control system is created in the MATLAB/Simulink platform, and the simulation and comparison analysis are carried out at low speed (3000r/min) and medium-high speed (8000r/min). The parameters of the BIM are shown in table 1.

The block diagram of rotor vibration suppression strategy presented in this paper is shown in Fig. 6. The whole control system consists of two subsystems: rotation and suspension parts. The rotation part is controlled by air-gap flux orientation. In the suspension part, the deviations between the given values and the actual values of the rotor displacements

TABLE 1. Parameters of the BIM.

Parameters	Torque winding	Suspension winding
Pole-pairs	1	2
Rotor outer diameter (mm)	97.8	97.8
Core length (mm)	105	105
Rotor mass (kg)	2.85	2.85
Rotational inertia (g • m^2)	7.96	7.96
Rated current (A)	2.86	2.86
Rotor resistance (Ω)	11.48	0.075
Stator resistance (Ω)	2.01	1.03
Rated power (w)	1000	500
Rotor leakage induction (mH)	9.22	5.42
Stator leakage induction (mH)	4.45	2.67
Mutual inductance of stator and rotor (mH)	158.56	9.32

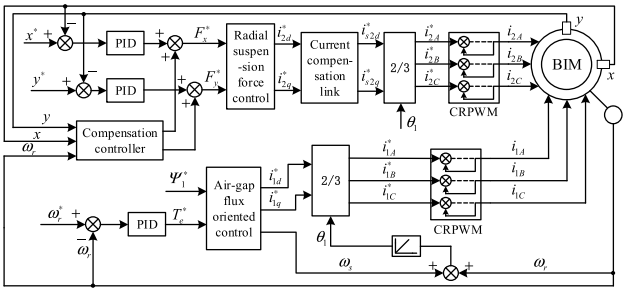

FIGURE 6. Block diagram of rotor vibration control for the BIM.

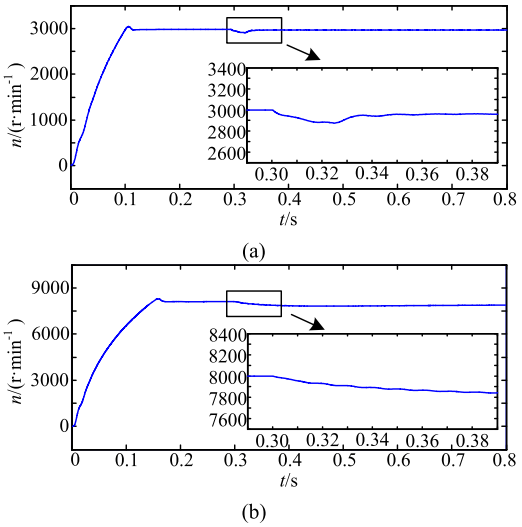

FIGURE 7. Speed response, (a) 3000r/min, (b) 8000r/min.

are adjusted by PID to obtain the radial suspension forces. Meanwhile, the compensation controller receives the rotor position information from the displacement sensor to generate the unbalanced compensation control force. The two forces are added to obtain the required suspension forces F_x^* and F_y^*. The specific construction method of the compensation controller is shown in Fig.4. Then, the stable and controllable suspension currents i_{s2d}^* and i_{s2q}^* are obtained through force/current conversion and current compensation. The specific construction method of the current compensation link is shown in Fig.5. Finally, the three-phase currents of the suspension winding are obtained by 2/3 transformation and CRPWM to control suspension windings. In the 2/3 transformation, θ_1 is the rotation transformation angle, which is obtained by integrating the sum of the slip angular velocity ω_s and the rotor angular velocity ω_1.

Fig.7 shows the speed response curves of the BIM at 3000r/min and 8000r/min. As shown in Fig.7(a), at low speed(3000r/min), the motor reaches a given speed at 0.11s, the speed response is fast and the overshoot is small. When the load is applied at 0.3 s, the speed is slightly decreased, but in a short time, the speed rises quickly and eventually reaches a steady state with little stability error. As shown in Fig.7(b), at medium-high speed(8000r/min), the motor reaches a given speed at 0.17s, and the speed response is slower than that at low speed. When the motor is suffered from the load at 0.3s, the speed is reduced in some extent and finally it becomes a remained constant after 0.1s. Overall, the compensation control system has good speed response characteristics at low speed and medium-high speed.

Fig.8 shows the rotor displacements of the BIM in the x, y directions with and without compensation. The speed is 3000r/min and the load is applied at 0.3s. As shown in Fig.8(a) and 8(c), without compensation, the rotor radial displacements have obvious unbalance fluctuation at the initial stage due to the rotor eccentricity and the vibration process lasts for a long time. At 0.3s, the rotor has a large vibration in the radial direction and it restores to normal after about 0.2s. As shown in Fig.8(b) and 8(d), with compensation, the rotor displacements are significantly improved, the displacement fluctuation is reduced after a sudden load and the recovery time is decreased to 0.12s, which indicates that the rotor vibration is effectively reduced.

Fig.9 shows the rotor displacements of the BIM in the x, y directions with and without compensation. The speed is 8000r/min and the load is applied at 0.3s. Compared with the rotor displacements at low speed, the vibration frequency and vibration amplitude of the rotor are visibly increased at medium-high speed. As shown in Fig.9, the amplitude of displacements with compensation is obviously lower than that without compensation, the amplitude and the oscillation period of rotor displacements are also improved after sudden load. Moreover, the fluctuation of displacements is smaller after stabilization and the suspension performance of the rotor is improved.

Fig.10 and 11 show the rotor trajectories at low speed (3000r/min) and medium-high speed (8000r/min), respectively. As shown in Fig.10 and 11, regardless of low speed or medium-high speed, the motion trajectory of the rotor is reduced in comparison with that under the condition of no compensation, and the time to reach the equilibrium position is shorter. In addition, due to the uneven distribution of rotor

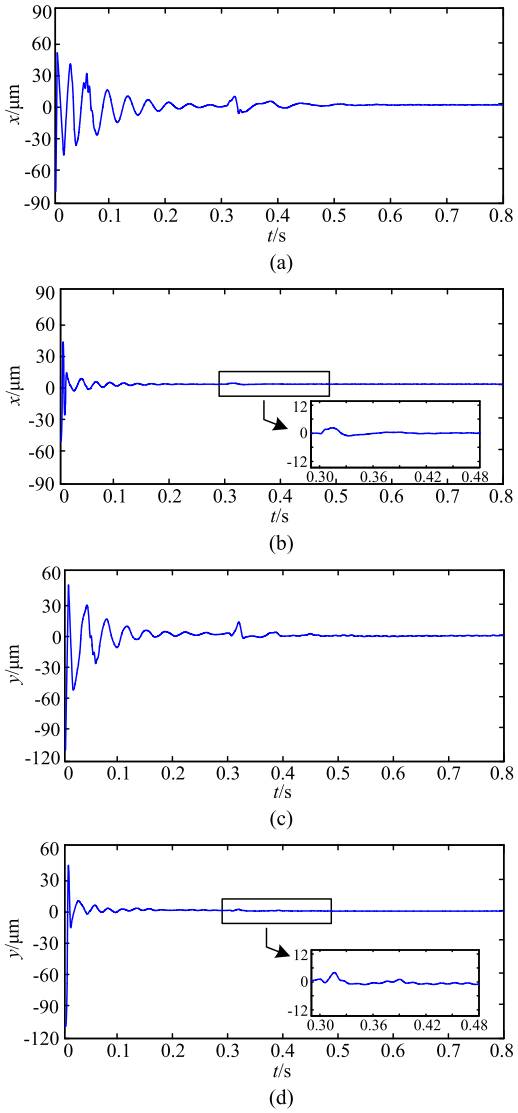

FIGURE 8. Rotor vibration suppression results at 3000r/min, (a) the radial displacement of the x-axis without compensation, (b) the radial displacement of the x-axis with compensation, (c) the radial displacement of the y-axis without compensation, (d) the radial displacement of the y-axis with compensation.

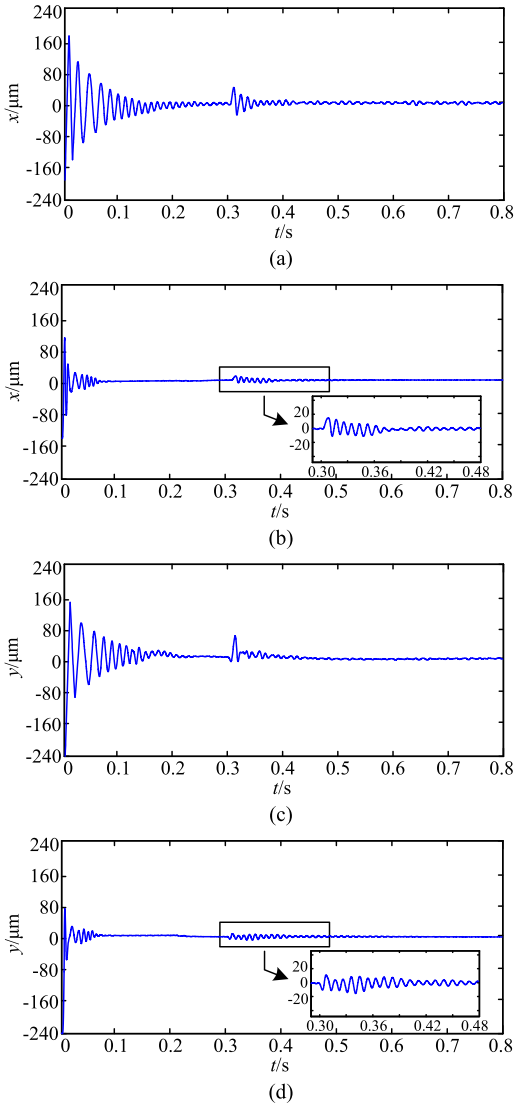

FIGURE 9. Rotor vibration suppression results at 8000r/min, (a) the radial displacement of the x-axis without compensation, (b) the radial displacement of the x-axis with compensation, (c) the radial displacement of the y-axis without compensation, (d) the radial displacement of the y-axis with compensation.

mass, the centrifugal force is larger at medium-high speed and the vibration is more severe. Comparing the two situations, the compensation effect is better under the condition of medium-high speed.

B. RESULTS AND ANALYSIS OF THE EXPERIMENT

To further verify the effectiveness of the proposed rotor vibration suppression strategy, a control system platform is established by utilizing a BIM as an experimental prototype. The BIM experimental platform is shown in Fig.12. The motor parameters in the experiment are the same as those in the simulation. Due to the limitation of the speed measured by photoelectric encoder, the given speed is set to 3000r/min. The three-phase AC voltage is 380V. In this experiment, photoelectric encoder and displacement sensor are used to

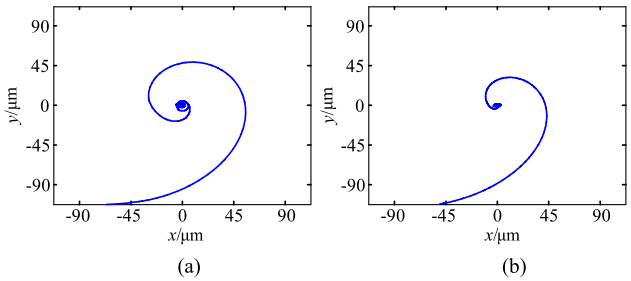

FIGURE 10. Trajectories of rotor operation at 3000r/min, (a) without compensation, (b) with compensation.

obtain the actual speed and rotor displacement respectively. Magnetic powder brake and load regulator are used to simulate and adjust the load respectively. The oscilloscope will

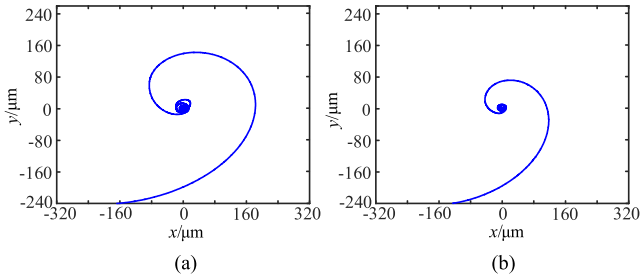

FIGURE 11. Trajectories of rotor operation at 8000r/min, (a) without compensation, (b) with compensation.

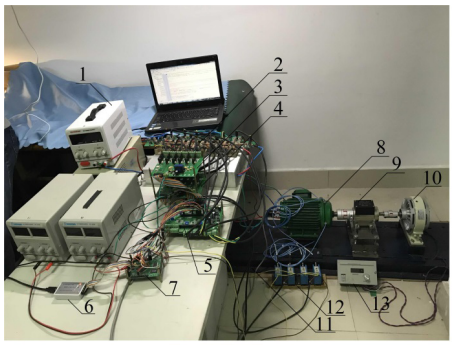

1. power supply; 2. inverter; 3. suspension winding control circuit; 4. torque winding control circuit; 5. control mainboard; 6. simulator; 7. DSP; 8. experimental prototype; 9. torque sensor; 10. load (magnetic powder brake); 11. bench; 12. displacement sensor; 13. load regulator

FIGURE 12. BIM experimental platform.

display the displacement waveform measured in the experiment. The motor starts at no load first. After the motor runs stably, the rotor radial displacement under stable state is measured, and then the sudden load is applied to the motor to obtain the rotor radial displacement under dynamic state. The results of the rotor vibration suppression experiment are shown in Fig.13-15.

Fig.13 shows the rotor radial displacements in two different conditions. As shown in Fig.13(a), the rotor displacements in the x, y directions without compensation are 45μm and 60μm, respectively. As shown in Fig.13(b), the rotor displacements in the x, y directions with compensation are 30μm. As can be seen from these two figures, the rotor displacements are significantly reduced after compensation, which indicates that the proposed compensation control strategy has a good vibration suppression effect under steady state conditions.

Fig.14 shows the rotor displacements with a sudden load. Comparing Fig.14(a) and Fig.14(b), it can be seen that the displacements in the x, y directions have different degrees of change after the load is applied. The time required for the rotor to return to the stable operation state without compensation is 90ms, while the rotor only needs 73ms to achieve steady state with compensation. Moreover, the amplitude of the disturbance is smaller, which demonstrates that the compensation strategy can effectively reduce the rotor

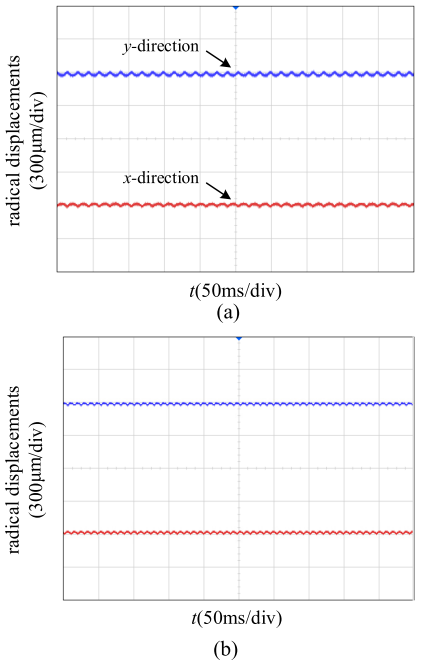

FIGURE 13. Rotor radial displacement at steady state, (a) Without compensation, (b) with compensation.

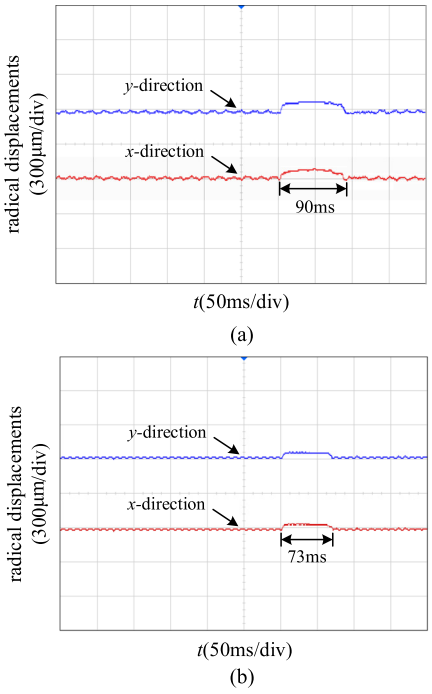

FIGURE 14. Rotor radial displacement under sudden load, (a) without compensation, (b) with compensation.

vibration under the dynamic condition and it also has good anti-disturbance performance.

Fig.15 shows the trajectories of the rotor centroid with and without compensation. Comparing Fig.15(a) and Fig.15(b), the maximum displacement of centroid trajectory without compensation is 80μm. The rotor centroid always moves

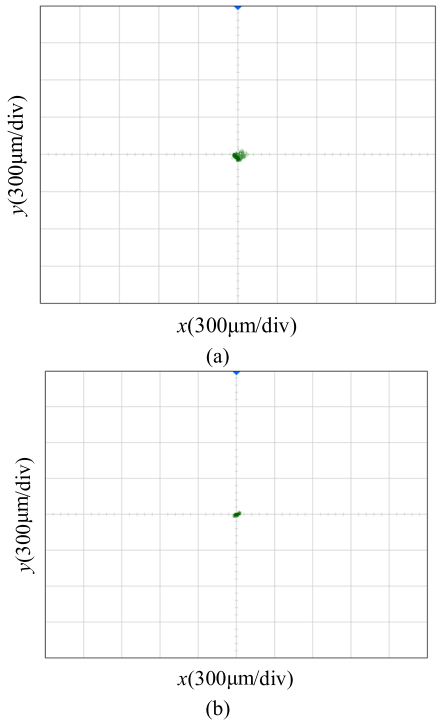

FIGURE 15. Trajectories of the rotor, (a) without compensation, (b) with compensation.

slightly along the central equilibrium position under the condition of compensation, and the trajectory is obviously reduced. In a word, Fig.15 illustrates that the rotor trajectory is effectively improved and the suspension performance is enhanced by the proposed compensation strategy.

VI. CONCLUSION

In this paper, based on the analysis of unbalanced vibration caused by the rotor eccentricity of the BIM, the dynamic model of the rotor vibration is derived. Meanwhile, the rotor vibration is reduced by means of the control strategy combined with the unbalanced force feed-forward compensation and current compensation, and the effectiveness of the proposed method for vibration suppression is verified by comparing the rotor displacements with and without compensation in simulation and experiment (including load mutation). The main conclusions can be summarized as follows.

1) The synchronous displacement signals detected by the displacement sensors are larger owing to the rotor eccentricity during the operation of the BIM, and the output unbalanced force will be accordingly increased after the adjustment of the controller. Moreover, the radial suspension force is affected in a certain extent due to the induced current of the suspension winding in the rotor, thus increasing the vibration amplitude of the rotor.

2) By comparing the rotor displacements with and without compensation, the proposed compensation control strategy has good control effects under different speeds and loads. It can effectively suppress the unbalanced vibration of the rotor under different operating conditions. Meanwhile, the vibration amplitude is obviously reduced and the trajectory of the rotor is improved. In addition, the strategy makes the control system have good dynamic and static performances and enhances the suspension precision of the rotor.

3) The experimental results show that when the motor speed is 3000r/min, the maximum radial displacement of the rotor with compensation is about half of that without compensation, which indicates the rotor vibration is effectively suppressed. Accordingly, the effectiveness of the proposed control strategy is verified. The experiment of the BIM at higher speed will be further studied in the future.

REFERENCES

[1] W. Bu, F. He, Z. Li, H. Zhang, and J. Shi, "Neural network inverse system decoupling control strategy of BLIM considering stator current dynamics," *Trans. Inst. Meas. Control*, vol. 41, no. 3, pp. 621–630, Feb. 2019.

[2] X. Sun, B. Su, L. Chen, Z. Yang, J. Chen, and W. Zhang, "Nonlinear flux linkage modeling of a bearingless permanent magnet synchronous motor based on AW-LSSVM regression algorithm," *Int. J. Appl. Electromagn. Mech.*, vol. 51, no. 2, pp. 151–159, Jun. 2016.

[3] X. Sun, C. Hu, G. Lei, Y. Guo, and J. Zhu, "State feedback control for a PM hub motor based on gray wolf optimization algorithm," *IEEE Trans. Power Electron.*, vol. 35, no. 1, pp. 1136–1146, Jan. 2020.

[4] E. Severson, S. Gandikota, and N. Mohan, "Practical implementation of dual purpose no voltage drives for bearingless motors," *IEEE Trans. Ind. Appl.*, vol. 52, no. 2, pp. 1509–1518, Apr. 2016.

[5] Z. Yang, J. Ji, X. Sun, H. Zhu, and Q. Zhao, "Active disturbance rejection control for bearingless induction motor based on hyperbolic tangent tracking differentiator," *IEEE J. Emerg. Sel. Topics Power Electron.*, to be published, doi: 10.1109/jestpe.2019.2923793.

[6] X. Cao, J. Zhou, C. Liu, and Z. Deng, "Advanced control method for a single-winding bearingless switched reluctance motor to reduce torque ripple and radial displacement," *IEEE Trans. Energy Convers.*, vol. 32, no. 4, pp. 1533–1543, Dec. 2017.

[7] W. Bu, Y. Huang, Z. Li, H. Shi, and J. Shi, "Diaplacement sensorless control strategy of bearingless induction motor," *Int. J. Appl. Electromagn. Mech.*, vol. 54, no. 4, pp. 597–610, Jul. 2017.

[8] A. Sinervo and A. Arkkio, "Rotor radial position control and its effect on the total efficiency of a bearingless induction motor with a cage rotor," *IEEE Trans. Magn.*, vol. 50, no. 4, pp. 1–9, Apr. 2014.

[9] X. Sun, Z. Shi, L. Chen, and Z. Yang, "Internal model control for a bearingless permanent magnet synchronous motor based on inverse system method," *IEEE Trans. Energy Convers.*, vol. 31, no. 4, pp. 1539–1548, Dec. 2016.

[10] X. Xu, J. Liu, and S. Chen, "Internal model control for reduction of bias and harmonic currents in hybrid magnetic bearing," *Mech. Syst. Signal Process.*, vol. 115, pp. 70–81, Jan. 2019.

[11] X. Sun, B. Su, S. Wang, G. Lei, and J. G. Zhu, "Performance analysis of suspension force and torque in an IBPMSM with V-shaped PMs for flywheel batteries," *IEEE Trans. Magn.*, vol. 54, no. 11, Nov. 2018, Art. no. 8105504.

[12] A. Chiba and J. A. Santisteban, "A PWM harmonics elimination method in simultaneous estimation of magnetic field and displacements in bearingless induction motors," *IEEE Trans. Ind. Appl.*, vol. 48, no. 1, pp. 124–131, Jan. 2012.

[13] V. F. Victor, F. O. Quintaes, J. S. B. Lopes, L. D. S. Junior, A. S. Lock, and A. O. Salazar, "Analysis and study of a bearingless AC motor type divided winding, based on a conventional squirrel cage induction motor," *IEEE Trans. Magn.*, vol. 48, no. 11, pp. 3571–3574, Nov. 2012.

[14] X. Sun, L. Chen, H. Jiang, Z. Yang, J. Chen, and W. Zhang, "High-performance control for a bearingless permanent-magnet synchronous motor using neural network inverse scheme plus internal model controllers," *IEEE Trans. Ind. Electron.*, vol. 63, no. 6, pp. 3479–3488, Jun. 2016.

[15] G. Valente, A. Formentini, L. Papini, C. Gerada, and P. Zanchetta, "Performance improvement of bearingless multisector PMSM with optimal robust position control," *IEEE Trans. Power Electron.*, vol. 34, no. 4, pp. 3575–3585, Apr. 2019.

[16] Y. Ren, X. Chen, Y. Cai, H. Zhang, C. Xin, and Q. Liu, "Attitude-rate measurement and control integration using magnetically suspended control and sensitive gyroscopes," *IEEE Trans. Ind. Electron.*, vol. 65, no. 6, pp. 4921–4932, Jun. 2018.
[17] X. Hu, F. Gao, C. Cui, J. Liu, H. Wang, Y. Li, Z. Ni, J. Cheng, and L. Yan, "Analysis of mass unbalance torque on a spinning superconducting rotor," *IEEE Trans. Appl. Supercond.*, vol. 24, no. 3, pp. 1–4, Jun. 2014.
[18] C. Peng, J. He, M. Zhu, Z. Deng, Z. Zhen, and Q. Liu, "Optimal synchronous vibration control for magnetically suspended centrifugal compressor," *Mech. Syst. Signal Process.*, vol. 132, pp. 776–789, Oct. 2019.
[19] C. Peng, J. He, M. Zhu, Z. Deng, Z. Zhen, and Q. Liu, "Three-dimensional identification for unbalanced mass of rotor systems in operation," *Appl. Sci.*, vol. 8, no. 2, p. 173, Jan. 2018.
[20] V. Mukherjee, P. Rasilo, F. Martin, and A. Belahcen, "Effect of magnetic forces and magnetostriction on the stator vibrations of a bearingless synchronous reluctance motor," *IEEE Trans. Magn.*, vol. 55, no. 6, pp. 1–4, Jun. 2019.
[21] J. Kejian, Z. Changsheng, and C. Liangliang, "Unbalance compensation by recursive seeking unbalance mass position in active magnetic bearing-rotor system," *IEEE Trans. Ind. Electron.*, vol. 62, no. 9, pp. 5655–5664, Sep. 2015.
[22] X. Xu, J. Liu, and S. Chen, "Synchronous force elimination in the magnetically suspended rotor system with an adaptation to parameter variations in the amplifier model," *IEEE Trans. Ind. Electron.*, vol. 65, no. 12, pp. 9834–9842, Dec. 2018.
[23] S.-M. Yang, "Electromagnetic actuator implementation and control for resonance vibration reduction in miniature magnetically levitated rotating machines," *IEEE Trans. Ind. Electron.*, vol. 58, no. 2, pp. 611–617, Feb. 2011.
[24] Q. Chen, G. Liu, and B. Han, "Suppression of imbalance vibration in AMB-rotor systems using adaptive frequency estimator," *IEEE Trans. Ind. Electron.*, vol. 62, no. 12, pp. 7696–7705, Dec. 2015.
[25] C. Peng, S. Zheng, Z. Huang, and X. Zhou, "Complete synchronous vibration suppression for a variable-speed magnetically suspended flywheel using phase lead compensation," *IEEE Trans. Ind. Electron.*, vol. 65, no. 7, pp. 5837–5846, Jul. 2018.
[26] W. Bu, Y. Huang, C. Lu, H. Zhang, and H. Shi, "Unbalanced displacement LMS extraction algorithm and vibration control of a bearingless induction motor," *Int. J. Appl. Electromagn. Mech.*, vol. 56, no. 1, pp. 35–47, Dec. 2017.
[27] S. Okubo, Y. Nakamura, and S. Wakui, "Unbalance vibration control for active magnetic bearing using automatic balancing system and peak-of-gain control," in *Proc. IEEE ICM*, Mar. 2013, vol. 307, no. 9, pp. 105–110.
[28] S.-R. Zhang, A.-G. Wu, and T.-H. Li, "Direct control for rotor eccentric displacement of bearingless permanent magnet-type synchronous motors," *Proc. Chin. Soc. Elect. Eng.*, vol. 27, no. 12, pp. 65–70, Apr. 2007.
[29] X. Qiao and C. Zhu, "The active unbalanced vibration compensation of the flexible switched reluctance motorized spindle," *J. Vib. Control*, vol. 20, no. 13, pp. 1934–1945, Oct. 2014.
[30] Q. Y. Zhang, Z. Q. Deng, and Y. Yang, "Compensation control of rotor mass eccentric in bearingless switched reluctance motors," *Proc. Chin. Soc. Elect. Eng.*, vol. 31, no. 21, pp. 128–134, Jul. 2011.
[31] S. Zhang, L. Liu, Y. Jia, S. Wang, and C. Qie, "Compensation control for radial suspension force in bearingless induction motors," in *Proc. IEEE 11th Conf. Ind. Electron. Appl. (ICIEA)*, Jun. 2016. pp. 2185–2189.
[32] H. Sugimoto, M. Miyoshi, and A. Chiba, "Axial vibration suppression by field flux regulation in two-axis actively positioned permanent magnet bearingless motors with axial position estimation," *IEEE Trans. Ind. Appl.*, vol. 54, no. 2, pp. 1264–1272, Mar. 2018.
[33] T. Zhang, W. Ni, and L. H. Mo, "Adaptive vibration-rejection control on permanent-magnet-type bearingless motors," *J. Vib. Shock.*, vol. 35, no. 20, pp. 65–70, Oct. 2016.
[34] Z. Yang, D. Dong, H. Gao, X. Sun, R. Fan, and H. Zhu, "Rotor mass eccentricity vibration compensation control in bearingless induction motor," *Adv. Mech. Eng.*, vol. 7, no. 1, Jan. 2015, Art. no. 168428.
[35] Z. B. Yang, D. W. Dong, X. D. Sun, and R. Fan, "Vibration compensation control of rotor mass eccentric in bearingless induction motor," *Chin. J. Sci. Instrum.*, vol. 36, no. 4, pp. 871–878, 2015.
[36] X. Sun, B. Su, L. Chen, Z. Yang, X. Xu, and Z. Shi, "Precise control of a four degree-of-freedom permanent magnet biased active magnetic bearing system in a magnetically suspended direct-driven spindle using neural network inverse scheme," *Mech. Syst. Signal Process.*, vol. 88, pp. 36–48, May 2017.
[37] E. A. De Freitas Nunes, A. O. Salazar, E. R. L. Villarreal, F. E. C. Souza, L. P. Dos Santos, J. S. B. Lopes, and J. C. C. Luque, "Proposal of a fuzzy controller for radial position in a bearingless induction motor," *IEEE Access*, vol. 7, pp. 114808–114816, 2019.
[38] W. S. Bu, S. M. Wan, S. H. Huang, and W. S. Liu, "General analytical model about controllable magnetic suspension force of bearingless motor," *Proc. Chin. Soc. Elect. Eng.*, vol. 29, no. 30, pp. 84–89, Oct. 2009.
[39] X. Sun, L. Chen, Z. Yang, and H. Zhu, "Speed-sensorless vector control of a bearingless induction motor with artificial neural network inverse speed observer," *IEEE/ASME Trans. Mechatronics*, vol. 18, no. 4, pp. 1357–1366, Aug. 2013.
[40] X. Ye, Z. Yang, and T. Zhang, "Modelling and performance analysis on a bearingless fixed-pole rotor induction motor," *IET Electr. Power Appl.*, vol. 13, no. 2, pp. 251–258, Feb. 2019.
[41] W. Bu, X. Zhang, and F. He, "Sliding mode variable structure control strategy of bearingless induction motor based on inverse system decoupling," *IEEJ Trans. Elect. Electron. Eng.*, vol. 13, no. 7, pp. 1052–1059, Jul. 2018.
[42] X. Sun, Y. Shen, Z. Zhou, Z. Yang, and L. Chen, "Modeling and control of a bearingless permanent magnet synchronous motor," *Int. J. Appl. Electromagn. Mech.*, vol. 53, no. 1, pp. 151–165, Jan. 2017.
[43] X. Sun, L. Chen, and Z. Yang, "Overview of bearingless induction motors," *Math. Problems Eng.*, vol. 2014, no. 1, pp. 1–10, Aug. 2014.
[44] W. Bu, Y. Chen, and C. Zu, "Stator flux orientation inverse system decoupling control strategy of bearingless induction motor considering stator current dynamics," *IEEJ Trans. Elect. Electron. Eng.*, vol. 14, no. 4, pp. 640–647, Apr. 2019.

HUIMIN ZHU was born in Nantong, Jiangsu, China, in 1994. She is currently pursuing the master's degree with Jiangsu University. Her main research direction is bearingless motors and their intelligent control technology.

ZEBIN YANG received the B.Sc., M.Sc., and Ph.D. degrees in electrical engineering from Jiangsu University, Zhenjiang, China, in 1999, 2004, and 2013, respectively. From 2014 to 2015, he was a Visiting Scholar with the School of Electrical, Mechanical, and Mechatronic Systems, University of Technology Sydney, Sydney, Australia. He is currently a Professor with Jiangsu University. His main research interests include drives and control for motors and magnetic levitation transmission technology.

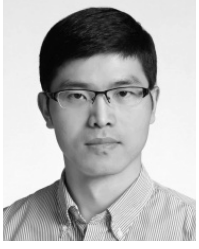

XIAODONG SUN (Senior Member, IEEE) received the B.Sc. degree in electrical engineering and the M.Sc. and Ph.D. degrees in control engineering from Jiangsu University, Zhenjiang, China, in 2004, 2008, and 2011, respectively. Since 2004, he has been with Jiangsu University, where he is currently a Professor with the Automotive Engineering Research Institute. From 2014 to 2015, he was a Visiting Professor with the School of Electrical, Mechanical, and Mechatronic Systems, University of Technology Sydney, Sydney, Australia. His current teaching and research interests include electrical machines and drives, drives and control for electric vehicles, and intelligent control. He is the author or coauthor of more than 80 refereed technical articles and one book. He is also the holder of 36 patents in his areas of interest.

DING WANG was born in Xuzhou, Jiangsu, China, in 1995. He is currently pursuing the master's degree with Jiangsu University. His main research direction is the bearingless induction motor and its intelligent control.

XI CHEN was born in Nantong, Jiangsu, China, in 1994. He is currently pursuing the master's degree with Jiangsu University. His main research direction is the bearingless induction motor and its intelligent control.